Geological, seismological and geodetic evidence of active thrusting and folding south of Mt. Etna (eastern Sicily): revaluation of "seismic efficiency" of the Sicilian Basal Thrust

Giorgio De Guidi[a], Graziella Barberi[b], Giovanni Barreca[a], Valentina Bruno[b],Fabrizio Cultrera[a], Sabrina Grassi[a], Sebastiano Imposa[a], Mario Mattia[b], Carmelo Monaco[a], Luciano Scarfì[b], Salvatore Scudero[a].

[a] Dipartimento di Scienze Biologiche, Geologiche e Ambientali, Sezione di Scienze della Terra, Università di Catania, Corso Italia 57, 95129 Catania, Italy. e-mail: deguidi@unict.it

[b] Istituto Nazionale di Geofisica e Vulcanologia, Osservatorio Etneo - Sezione di Catania, Piazza Roma, 2, 95123 Catania, Italy

ABSTRACT

Geological studies and morphological analysis, compared with seismological and geodetic data, suggest that a compressive regime currently occurs at crustal depth in the western sector of Mt. Etna, accommodated by shallow thrusting and folding at the front of the chain, south of the volcanic edifice. In particular, a large WSW-ENE trending anticline, interpreted as detachment fold, is growing west and north of Catania city (the Catania anticline). Geological data suggest that during the last 6000 years the frontal fold has been characterized by uplift rates of~6 mm/yr along the hinge, consistent with the interferometric data (10 mm/yr) recorded in the last 20 years. Moreover, a NNW-SSE oriented axis of compression has been obtained by seismological data, consistent with GPS measurements over the last 20 years which have revealed a shortening rate of ~5 mm/yr along the same direction. Besides the activity related to the volcanic feeding system, the seismic pattern under the Mt. Etna edifice can be certainly related to the regional tectonics. The compressive stress is converted into elastic accumulation and then in earthquakes along the ramps beneath the chain, whereas on the frontal area it is accommodated by aseismic deformation along an incipient

detachment within the clayish foredeep deposits. The high rate of shortening at the aseismic front of the chain, suggests a greater "seismic efficiency" in correspondence of ramps at the rear.

1. INTRODUCTION

In the Mt. Etna area two distinct tectonic domains, characterized by compressive and tensional regimes, coexist (Cocina et al., 1997; Palano et al., 2012).The eastern sector is characterized by shallow seismicity originating from normal-oblique faulting (the Timpe fault system; Fig. 1), related to WNW-ESE regional extension (Monaco et al., 1997; Monaco and Tortorici, 2000). Conversely, in the western sector, the distribution of earthquakes shows a clear deepening of foci moving from the southern border of the volcanic edifice towards the NNW, where compressive mechanisms mostly occur (20 and 30 km see Scarfi et al., 2013). Contractional structures outcrop south of the volcanic edifice and are represented by a W-E trending fold belt that have deformed Pleistocene terrigenous deposits in response of NNW-SSE oriented regional compression (Labaume et al., 1990; Catalano et al., 2011; Ristuccia et al., 2013).

Seismological (Neri et al., 2005) and geodetic (Mattia et al., 2012) data and in situ stress measurements (Ragg et al., 1999) confirm the occurrence of a still active compressional regime south of Mt. Etna, accommodated by thrusting and folding. In particular, new interferometric data recorded in the last 20 years, depict a large anticline (named the "Catania anticline") aseismically uplifting at a rate of ~10 mm/yr in the western and northern outskirts of Catania city (Lundgren et al., 2004; Bonforte et al., 2011). In order to verify if this aseismic frontal folding can be related to regional processes, characterized by convergence rates of about 5 mm/yr (Mattia et al., 2012), in this work we have analyzed crustal seismicity, geological field information and morphometric data obtained by 2x2m grid resolution DEM. Moreover, with the aim of verifying if strain accumulation is presently occurring on the growing anticline, we surveyed some benchmarks of a GPS network of the Italian Military Geographical Institute, realized in 1994 for cartographic and geodetic purposes.

2. GEOLOGICAL SETTING

The geodynamic setting of eastern Sicily (Fig. 1) is characterized by the Neogene-Quaternary flexure of the African-Pelagian continental paleo-margin beneath the SSE-verging Sicilian chain, culminating in the south-eastern sectors of the island to form the Hyblean Plateau, the foreland domain (Ben Avraham et al., 1990). Northwards, the foreland crust deepens under the chain. (Lavecchia et al., 2007and reference therein) between the northern coast of Sicily and Mt. Etna (Fig. 2). To the east, the offshore Malta Escarpment, a Mesozoic discontinuity partially reactivated in the late Quaternary, separates the continental crust of the Pelagian Block from the oceanic crust of the Ionian Sea (Bianca et al., 1999 and references therein). In such a geodynamic context, the area between the southern edge of the Mt. Etna volcanic edifice and the Hyblean Plateau (the Catania Plain) represents the remnant of a foredeep domain, filled by Pleistocene sediments and volcanics, and by Holocene alluvial-coastal deposits (Torelli et al., 1998). This sedimentary succession is mostly deformed by an asymmetric middle-late Pleistocene south-facing anticline, about 10 km long and ~W-E trending (the "Terreforti anticline", Labaume et al., 1990; Ristuccia et al., 2013) and other minor folds (Catalano et al., 2011) (Fig. 1). They have been interpreted as thrust propagation folds at the front of the chain, related to the migration of the thrust belt, as a response to the regional NNW-SSE compressive tectonic regime (Palano et al., 2012).

According to Lavecchia et al. (2007) the western and southern sectors of Mt. Etna are part of a unique regional-scale, northwards deepening crustal seismogenic structure (named Sicilian Basal Thrust SBT) whose focal mechanisms are compatible with a nearly N–S shortening and with some field evidence of active folding-and thrust deformation at the Sicilian chain front. In the north-western sector of the volcano the earthquakes reach a maximum depth of about 35 km. The analysis of fault plane solutions (e.g., Cocina et al., 1997; Patanè and Privitera, 2001; Scarfì et al., 2013) indicates that at the shallow and intermediate levels (down to 5 and 10 km, respectively), the stress field is influenced by the deep magmatic system of the volcano. Conversely, at greater depths, the regional dynamics is the main driving force with the P-axes being NW-SE oriented. This is

consistent with the regional pattern characterizing central and western Sicily (Sgroi et al., 2012), related to the Africa-Europe convergence (Hollenstein et al., 2003; Serpelloni et al., 2007; Caporali et al., 2009; Palano et al., 2012). The compressive domain coexists with the ESE-WNW extensional regime that produces the coseismic oblique-normal faulting, fracturing and sliding of the eastern flank of the volcano (Azzaro et al., 2013).

GPS velocity fields (Ferranti et al., 2008; Mattia et al., 2012), seismological (Lavecchia et al., 2007) and interferometric synthetic aperture radar data (Bonforte et al., 2011) suggest that contractional processes related to the migration of the thrust belt are still active and cause the growth of the "Catania anticline" in the western and northern outskirts of the town. Fold structures outcropping south of Mt. Etna have also been interpreted as the result of the gravitational spreading of the volcanic edifice of Mt. Etna over the sedimentary substratum (Borgia et al., 2000; Solaro et al., 2011; Bonforte et al., 2011). Current tectonic activity is also responsible for the destructive historical earthquakes ($M \geq 7$) that occurred in south-eastern Sicily (e.g. 1169 AD, 1693 AD events; Boschi et al., 1995). The location of seismogenic sources is a topic still widely debated: normal faults located along the Ionian offshore, where the Malta Escarpment has been reactivated since the middle Pleistocene (see Bianca et al., 1999 and references therein), and/or compressional structures between the front of the chain and the northern margin of the Hyblean foreland (see DISS Working Group, 2010).

3. SEISMICITY

The seismicity occurring in the crust beneath Mt. Etna, between the front of the Sicilian chain and the margin of the Hyblean foreland, was analysed by using a seismological dataset from the "Catalogo dei Terremoti della Sicilia Orientale - Calabria Meridionale," (Gruppo Analisi Dati Sismici, 2015) (Fig 1b).In particular, in the area of interest, the southern and western sectors of the volcano, selected data consist of about 1900 earthquakes, with small-to moderate-magnitude ($1.0 \leq M_L \leq 4.8$), recorded in 1999-2012 period through the INGV local network. Events located in the

105 eastern sector are not considered in our analysis, since most of them can be related to the shallow
106 extensional structures controlling the seaward Mt. Etna deformation pattern (see e.g. Alparone et
107 al., 2013; Azzaro et al., 2013 and references therein). Accurate hypocentres were obtained by
108 relocating the events by using a 3D velocity model (Patanè et al., 2006 and Chiarabba et al., 2004
109 for the deeper layers) and the software tomo DDPS (Zhang et al., 2009), which, by the combination
110 of both absolute and relative arrival time readings between couple of events of an earthquake
111 cluster, is able to produce sharp images of studied fault structures (see e.g., Gambino et al.,
112 2004;Alparone et al., 2012). The tomo DDPS hypocentral locations resulted in a 50% reduction in
113 the absolute RMS residual, if compared to the original ones, with almost 67% and 89% of events
114 having a final RMS smaller than 0.05 and 0.06 s, respectively. The average location uncertainties
115 are of about 0.20±0.08 km and 0.20±0.10 km in the horizontal and vertical directions, respectively.
116 Looking at the distribution of the earthquakes (Figs.1 and 2), a clear trend of the seismic events
117 deepening from very shallow hypocenters in the area south of Mt. Etna, is evident down to a depth
118 of about 35 km to the NNW. Most of the events are clustered in several groups. A first cluster of
119 earthquakes is found in the area west of the craters; it forms an earthquake cloud vertically
120 elongated from 0 to about 12 km of depth and slightly dipping northward. Another significant event
121 cloud is located about 10 km south of the craters at 10-15 km of depth (Figs.1 and 2), whereas the
122 deeper events (20-30km) and those with the highest magnitude ($M_L \geq 3.8$)occurred in the northern
123 sector of the volcano.
124 With the aim of characterizing the displacement type of the main seismogenic sources and the
125 stress field acting in the area, we computed focal mechanisms for the major and best recorded
126 earthquakes (Fig. 3), using first motion polarities and the FPFIT code of Reasenberg and
127 Oppenheimer (1985). After discarding fault plane solution not matching minimum quality criteria
128 (i.e. large uncertainties in the focal parameters), we collected 184 well-constrained focal
129 mechanism, in majority strike-slip or oblique type (60%), and several normal or thrust faults. A
130 careful analysis of the direction of the principal stress axes (P- and T-axes) revealed that the

seismogenic sources in the various crustal sectors beneath the volcano are characterised by different patterns (Fig.3). In particular, the cluster located west of the craters shows P-axes striking mostly about WNW-ESE (Fig 3a). Southward, earthquakes at 10-15 km of depth have P-axes quite uniformly NE-SW oriented (Fig.3b). Finally, fault mechanisms of the deeper events, to the north, show nearly horizontal P-axes striking NW-SE (Fig.3c).

The integrated analysis of seismic sources can discriminate and characterise crustal blocks by supplying information on the acting stress fields (Wyss et al., 1992). To this purpose a standard numerical technique (Gephart and Forsyth, 1984; Gephart, 1990), based on the inversion of the focal solutions, was applied to determine the shape of the stress ellipse(σ_1, σ_2, σ_3, the maximum, intermediate and minimum compressive stresses, respectively). The method identifies the best stress tensor model that most closely matches all the fault plane solutions considered in a source region, requiring as basic assumption that the stress is uniform in space and time domains in the investigated volume. A variable misfit (F), given by the angular difference between the observed slip direction on a fault plane and the shear stress derived from the stress model, provides a guide to how well the assumption of stress homogeneity is fulfilled (Michael, 1987). Following Wyss et al. (1992) and Gillard et al. (1996), we can assume that the condition of a homogeneous stress distribution is fulfilled if the misfit is smaller than 6° and that it is not fulfilled if $F > 9°$; for F values between 6° and 9° the solution is considered acceptable, but it may reflect some heterogeneities.

P-axes distribution clearly indicate that the stress field acting in the whole investigated volume is unlikely to be considered uniform. Therefore, we searched for sub-volumes where stress is uniform and well constrained, by inverting FPSs subsets corresponding to spatial partitions of the study region and evaluating the degree of stress heterogeneity in each subset by the analysis of the F-value. The most significant results are reported in Fig 4 and Tab 1, which display the sub-volumes and the earthquakes identified in our search for uniform stress domains and the corresponding orientation of the main stress axes. In particular, we identified three areas characterised by a strike-

157 slip regime with different orientation: i) in the deeper northern volume there is a sub-horizontal σ_1
158 striking NNW-SSE; ii) the central sector, between 0 and 9 km of depth, is characterized by a σ_1
159 striking E-W and iii) the southern volume, between 10 and 15 km of depth, is characterized by a σ_1
160 striking NE-SW. For the southern area, where the shallower earthquakes occur, no homogeneous
161 stress tensor has been obtained. Ultimately, our analysis reveals that at the shallower and
162 intermediate levels (down to 10-15 km), the seismicity is related to local processes, likely
163 influenced by the magmatic system of the volcano, while, at greater depths, the regional dynamics
164 is the main driving force with the stress NW-SE oriented (see also Scarfì et al, 2013).
165
166 **4. GPS DATA**
167 In 1992 the Italian IGMI (Istituto Geografico Militare Italiano - www.igmi.org) started the GPS
168 measuring of a network made up of 1260-bechmarks, extended over the whole Italian area. The
169 main target of this network was the cartographic framing of the Italian territory.
170 We re-surveyed three of these IGMI benchmarks north and south of the Catania Anticline (Figs.
171 1 and 5) in order to calculate the velocities of some benchmarks very close to the alignment
172 revealed by SAR data (Bonforte et al., 2011). The GPS survey was carried out by using Leica
173 GX1220 receivers and AR10 antennas, while instruments used by the IGMI in 1994 were Trimble
174 4000 SSE receivers and Trimble compact with ground plane (model 22020-00) antennas. GPS data
175 have been processed using the GAMIT/GLOBK software (Herring et al. 2006) with IGS
176 (International GNSS Service) precise ephemerides and Earth orientation parameters from the IERS
177 (International Earth Rotation Service). We framed the measurements to an external global reference
178 frame by including in our analysis the data from five GPS stations belonging to the IGS and EURA
179 networks and operating since 1994 (GRAZ, HERS, JOZE, MADR, ZIMM; see Palano et al., 2010
180 for location). The quasi-observations were then combined with global solutions (IGS1, IGS2,
181 EURA) provided by the Scripps Orbital and Permanent Array Center (SOPAC) at UC San Diego.
182 The loosely constrained daily solutions were transformed into ITRF2005 (2005 International

183 Terrestrial Reference Frame (Altamimi et al., 2007) and then rotated into a fixed Eurasia frame.

184 The obtained velocity field shows that the two GPS stations south of the anticline (UNIG, S114)
185 move with velocities of about 4 mm/yr along NNW to NNE directions, whereas the station located
186 north of the structure (TIRI) move to the SSW with velocity of about 2 mm/yr. These results are
187 consistent with NNW-SSE vectors obtained by permanent stations (Mattia et al., 2012), related to
188 the Africa-Europe convergence process, with the exception of the TIRI benchmark that could be
189 affected by the dynamics of the volcano (inflation/deflation processes; e.g. Bruno et al., 2012).
190 Accordingly, the volcano acts as a buttress to the propagation of ground deformation related to
191 tectonic processes. Recently Cianetti et al. (2012) applied a numerical model to calculate
192 normalized horizontal and vertical displacements for analytical models of magmatic sources and
193 from this analysis is possible to deduce that benchmarks placed at distance of 20-25 km from the
194 craters (e.g. TIRI) are potentially still affected by the action of the inflation/deflation cycles typical
195 of the discharge/recharge process of an active volcano, while increasing this distance the effects are
196 negligible (e.g. UNIG, S114).

197

198 ## 5. MORPHOSTRUCTURAL DATA

199 New field surveys were performed with the aim to verify if ground deformation provided by
200 satellite data is consistent with geological and morphological features. The fold axis of the Catania
201 anticline is located in a volcanic and strongly populated area (Fig. 6). So, field evidence of active
202 thrusting and folding is difficult to observe. However, results indicate that the differential ground
203 motion provided by interferometric data matches with morphostructural field data, which clearly
204 suggest active vertical deformation. The geological section (A-A' in Fig.7b) the fold axis (Bonforte
205 et al., 2011; field geology from Monaco et al.,2000; Monaco et al., 2010; Branca et al., 2011; 2x2 m
206 grid DEM from www.sitr.regione.sicilia.it/pai) shows the paleo-morphology of the Pleistocene
207 sedimentary substratum, characterized by ''pre-Etnean clays'' and by coastal-alluvial terraces
208 whose formation is related to the interplay between eustatic sea level changes and the tectonic

vertical movements during the last200 ky (Monaco et al. 2002). The lava covers, the oldest dating back to about 6,000 years ago Branca et al., 2011), have sealed the natural hydrological and weathering surface processes from then on. The section intersects crosswise a series of paleo valleys and drainage divides, carved on the paleo-landscape. The peculiar features of the mature landscape (soft shape, U valley with gentle slopes) represent the paleo-morphology of a substratum buried by invasion of lava flows. The lengthwise section also shows the convex shape of the envelope line of the substratum, with a maximum vertical uplift of 40 m halfway of the fold axis (section A-A' in Fig. 7b). The upper envelope line of topography mimics and progressively converges halfway with the previous one. The lava covers generally flowed with roughly N-S direction to the lower southern slope of the volcano, only the latest ones (since 4 ka ago, Branca et al., 2011) showing deflection in proximity of the deformed belt (Fig.6).

The morphometric analysis of drainage basins was also carried out. The hydrological basins of Cardinale, Cubba, Rosa, Sieli, Motta and Finaita "consequent" rivers (Fig. 7a), are characterized by N-S oriented elongated shape, straight trajectories, and surface areas of 6÷14 km^2 (Tab. 2). The basin heads appear to interact with the active deformation zone. As regards the basin shape, the Eb strength index represents the measure of the elongation of a basin (Schumm, 1956). The results (Tab.2) indicate very low values of Eb index, with limited changes (Strahler 1964).The analysis of hypsometric curves has been also performed. Differences in hypsometric curves are related to the variability of the geomorphic processes that shape the landscape (Fig.7b). So, they are used to discriminate different areas affected by vertical deformation and consequent erosional processes (Pike and Wilson, 1971; Mayer, 1990). The hypsometric curve of Finaita catchment shows uplifted low energy paleo surfaces strongly eroded by the river. It is worth noting the presence of inflections in the other curves.

6. DATA ANALYSIS

Interferometric data, recorded in the last 20 years (Lundgren et al., 2004; Bonforte et al., 2011), depict a large anticline in the western and northern outskirts of the town (the "Catania anticline"), aseismically uplifting at a rate of ~10 mm/yr along the hinge. GPS measurements indicate that the present-day shortening rate, accommodated by the fold, is about 5 mm/yr along NNW-SSE direction. Our geological and morphological analyses highlight that either sedimentary substratum and topographic relief have been recently affected by antiformal deformation in response to NNW-SSE shortening. The Eb index obtained by morphometric analysis of the drainage basins located south-west of the deformed area indicates that they are at rather juvenile stage and that the erosional activity, compensate the tectonic uplift . Inflections in the hypsometric curves indicate local uplift effects. The N-S orientation of consequent streams, whose headwaters appear to interact with the active deformation zone, also suggest the recent activity of the Catania anticline. The progressive convergence of the reconstructed marker lines toward the middle part of the fold (see section A-A' in Fig. 7b) suggests that the deformation has been coeval with the lava invasion. The sedimentary substratum is characterized by mature landscape that hasn't recorded the erosional effects induced by uplift processes having been sealed by lava flows since about 6000 years ago. Moreover, the youngest lava flows seem to be deflected by the growing antiform. The longitudinal section of Fig. 7b shows a maximum vertical deformation of 40 m along the hinge zone, suggesting a vertical uplift rate of about 6 mm/yr in the last 6000 yr,, which is consistent with the interferometric and GPS data.

The rapid growth of the fold would presuppose the existence of an active thrust at depth, related to the migration of the chain front. Seismological data show a clear trend of seismic events, characterized by shallow hypocenters in the area south of Etna, deepening to a depth of about 35 km to the NNW. They also confirm that at the shallower and intermediate levels (down to 10-15 km), the stress field is inevitably influenced by the deep magmatic system of the volcano, while, at greater depths, the NNW-SSE oriented stress is the main driving force related the regional

dynamics (see also Scarfì et al, 2013). The seismic dataset also gives us the opportunity to compare the percentage of the brittle deformation with respect to the observed geodetic and geologic strain. With this aim, magnitudes of the selected earthquakes were converted into scalar moments through the relationship proposed for the considered area by Giampiccolo et al. (2007). Averaging the value for the whole considered period (1999-2012), the estimated seismic moment resulted in1.74*10^15 N*m/yr. To compute the total amount of slip represented by the seismic activity we used the Brune (1968) relation:

$$Su = SM_0/mA_0$$

where u is the average dislocation of the shear surface, M_0 is the seismic moment, m is the shear modulus of faulted rock (assigned 2.8*10^10 N/m^2) and A_0 is the total area of the shear zone. The real areal extension of the shear zone is not well constrained: even though the seismogenic thickness is 35 km and the average dip angle 45°, the length of shear zone could be extended westwards, as suggested by morphometric and morphostructural data (Fig. 1 and 7). The slip rate is calculated dividing the total amount of slip for the temporal interval of recorded earthquakes. Taking into account the above mentioned uncertainty, the obtained values of seismic slip rate range from 0.25 to 0.38 mm/yr, that is one order of magnitude lower than the values estimated by geodetic and geological data.

This deficit could indicate either a proportion of aseismic deformation or overdue earthquakes. However, some key elements must be taken into account to explain this discrepancy, such as a poorly defined geometry of the modelled tectonic structure and the limited seismic catalog, understood as the recording time. In fact, during the considered seismic period any relevant earthquake occurred in the analysed area. Conversely, in the last 200 years several moderate and strong earthquakes have been associated to a seismogenic source compatible, for geometry and dimension, with the Catania compressive front: 1693 (M=7.0), 1818 (M=6.2), 1848 (M=5.5), and 1959 (M=4.7) (Azzaro and Barbano 2000; Barbano and Rigano 2001). Accordingly, the high level of seismicity in the past can account for the current low seismic rate. Anyhow, great caution is

287 required in interpreting these results, due to the narrow-data and the associated uncertainty. On the
288 other hand, we observe that the considered seismic data set is distributed in the whole crustal
289 thickness (~35 km), but approaching the front of the Sicilian thrust and fold belt shallow seismicity
290 (<5 km) is almost totally lacking. Hence, the seismic slip rate calculated by earthquake moments
291 can be associated to the whole crustal volume, while the values obtained by geodetic measurements
292 and geological estimation are related to shallower structural levels. Moreover, the effect of a
293 shallower source of deformation (e.g. inflation/deflation processes related to volcanic dynamics),
294 able to account for a portion of the missing rate, cannot be excluded, as demonstrated by the TIRI
295 benchmark.

296 Indeed, data on the geometric relationships between the growing anticline and the underlying
297 tectonic structure (eg. seismic profiles), potentially accommodating seismogenic deformation, are
298 lacking. Taking into account the relationships between thrusts and the overlying anticlines, thrust-
299 related anticlines can be described by three end-member geometries (Storti and Poblet, 1997): fault-
300 bend folding, fault-propagation folding, and decollement or detachment folding. Combining the 5
301 mm/yr shortening across the anticline with the 10 mm/yr of corresponding uplift, the hypothetical
302 slip on a unique shear surface would result on a >60° dipping plane. Such attitude is unrealistic for a
303 thrust or for a ramp, therefore the fault-propagation folding or the fault-bend folding models should
304 be excluded. Conversely, kinematic models have shown that detachment fold model can account for
305 uplift rate greater than shortening, in particular in the early stages of the anticline growth (Fig. 8).
306 Several examples of deformation at chain fronts, with similar strain rates (from GPS and
307 interferometry), have been related to shallow detachment and related folding (Huang et al., 2006;
308 Nishimura et al., 2008; Belabbes et al. 2009). We propose the occurrence of an incipient
309 decollement folding at the chain front, as response of a shallow detachment thrust migrating within
310 the clayish deposits of the foredeep or at the top of the buried foreland sequence. This structure is
311 clearly showed by seismic profiles southwards (see Torelli et al., 1998).

312

7. CONCLUSIONS

Geological and morphological analyses, compared with seismological and geodetic data, suggests that a compressive regime currently occurs at crustal depth in the western sector of Mt. Etna, accommodated by shallow thrusting and folding at the front of the chain, south of the volcanic edifice. Active tectonics in this part of the Sicilian fold-and-thrust belt are mainly controlled by the ~NNW-SSE compression caused by the Nubia – Eurasia convergence. The orientation of the P-axes at depth > 10 km, where seismogenic processes related to the volcano activity can be considered less relevant, and the geological evidence at surface are both consistent with these regional dynamics. It's worth noting that at shallow crustal level the inflation/deflation processes could act as a buttress to the underthrusting of the Hyblean slab, amplifying the shortening rate. The seismicity distribution and the slip rate velocities indicate a coexistence and interaction of thick and thin-skinned deformation across this domain. The basement is involved in crustal thrusting along relatively high-angle shear zone (the SBT; Lavecchia et al., 2007), while the frontal and shallow part of the belt is affected by low-angle blind thrust sand detachment folds (Figs. 2 and 8).

In conclusion, besides the activity related to the volcanic feeding system, the seismic pattern under Mt. Etna edifice can be certainly related to the regional dynamics. The compressive stress is converted into elastic accumulation and then in earthquakes along the ramps to the rear of the chain, whereas along the frontal flat it is accommodated by aseismic ductile deformation along an incipient detachment within the clayish foredeep deposits. In fact, despite the high rates of convergence, the seismicity is moderate at the front of the chain and the "seismic efficiency" of the SBT is greater in correspondence of ramps at the rear, where strong earthquakes can occur. Although the geodetic data show that strong shortening is localized in the eastern sector of the Sicilian chain front (see also Ferranti et al., 2008; Mattia et al., 2012 Musumeci et al., 2014), nonetheless active thrusting along the SBT has been also documented in western Sicily, where strong earthquakes occurred in historical times (Monaco et al., 1996; Barreca et al., 2014). This suggests that the thrust-and-fold system is not active simultaneously all along the Sicilian chain

front, but episodes of high deformation may occur in different segments of the SBT over time, implying the necessity of a better evaluation of the seismic hazard of this area.

ACKNOWLEDGEMENTS

This work was funded by a DPC-INGV 2012 grant, Project V3 "Multi-disciplinary analysis of the relationship between tectonic and volcanic activity" and by PRIN 2010-11 Project “Active and recent geodynamics of Calabrian Arc and accretionary complex in the Ionian Sea” (responsible C. Monaco).

347 **REFERENCES**

348 Alparone, S., Barberi, G., Cocina, O., Giampiccolo, E., Musumeci, C. , Patanè, D., 2012. Intrusive
349 mechanism of the 2008-2009 Mt. Etna eruption: Constraints by tomographic images and stress
350 tensor analysis. J. Volc. Geotherm. Res. 229-230, 50-63.

351 Alparone, S., D'Amico, S., Gambino, S., Maiolino, V., 2013. Buried active faults in the Zafferana
352 Etnea territory (south-eastern flank of Mt. Etna): geometry and kinematics by earthquake
353 relocation and focal mechanisms. Ann. of Geophys. 56, 1, doi:10.4401/ag-5758.

354 Altamimi, Z., Collilieux, X., Legrand, J., Garayt, B., Boucher, C. , 2007. ITRF2005: A new release
355 of the International Terrestrial Reference Frame based on time series of station positions and
356 Earth Orientation Parameters. J. Geophys. Res. 112, B09401.

357 Azzaro, R., Barbano, M. S., 2000. Analysis of the seismicity of Southeastern Sicily: a proposed
358 tectonic interpretation. Ann. of Geophys. 43, 1.

359 Azzaro, R., Bonforte, A., Branca, S., Guglielmino, F., 2013. Geometry and kinematics of the fault
360 systems controlling the unstable flank of Etna volcano (Sicily). J. Volc. Geotherm. Res. 251, 5–
361 15.

362 Barbano, M.S., Rigano, R., 2001. Earthquake sources and seismic hazard in Southeastern Sicily.
363 Ann. of Geophys. 44, 4.

364 Barreca, G., Bruno, V., Cocorullo, C., Cultrera, F., Ferranti, L., Guglielmino, F., Guzzetta, L.,
365 Mattia, M., Monaco, C., Pepe, F., 2014. Geodetic and geological evidence of active tectonics in
366 south-western Sicily (Italy). J. Geodynamics 82, 138–149, doi:10.1016/j.jog.2014.03.004.

367 Belabbes, S., Meghraoui M., Çakir Z., Bouhadad Y., 2009. InSAR analysis of a blind thrust rupture
368 and related active folding: the 1999 Ain Temouchent earthquake (Mw 5.7, Algeria) case study. J.
369 of Seismol. 13, 421–432, Doi:10.1007/s10950-008-9135-x.

370 Ben-Avraham, Z., Boccaletti, M., Cello, G., Grasso, M., Lentini, F., Torelli, L., Tortorici, L., 1990.
371 Principali domini strutturali originatisi dalla collisione neogenico-quaternaria nel Mediterraneo
372 centrale. Mem. Soc. Geol. It. 45, 453–462.

373 Bianca, M., Monaco, C., Tortorici, L., Cernobori, L., 1999. Quaternary normal faulting in
374 southeastern Sicily (Italy): a seismic source for the 1693 large earthquake. Geophys. J. Int, 139,
375 370-394.
376 Bonforte, A., Guglielmino, F., Coltelli, M., Ferretti, A., Puglisi, G., 2011. Structural assessment of
377 Mount Etna volcano from Permanent Scatterers analysis. Geoch. Geophys. Geosyst. 12, Q02002,
378 doi:10.1029/2010GC003213.
379 Borgia, A., Lanari, R., Sansosti, E., Tesauro, M., Berardino, P., Fornaro, G., Neri, M., Murray, J.B.,
380 2000. Actively growing anticlines beneath Catania from the distal motion of Mount Etna's
381 decollement measured by SAR interferometry and GPS. Geophys. Rese. Lett. 27(20), 3409–
382 3412.
383 Boschi, E., Ferrari, G., Gasperini, P., Guidoboni, E., Smriglio, G.,Valensise G., 1995. Catalogo dei
384 forti terremoti in Italia dal 461 a.C. al 1980. ING-SGA, Bologna, 973 pp.
385 Branca, S., Coltelli, M., Groppelli, G., Lentini, F., 2011. Geological map of Etna volcano, 1:50,000
386 scale. Ital. J. Geosci. 130 (3), 265–291, http://dx.doi.org/10.3301/IJG.2011.15.
387 Brune, J. N., 1968. Seismic moment, seismicity, and rate of slip along major fault zones. J.
388 Geophys. Res. 73(2), 777-784.
389 Bruno, V., Mattia, M., Aloisi, M., Palano, M., Cannavò, F., and Holt, W. E., 2012. Ground
390 deformations and volcanic processes as imaged by CGPS data at Mt. Etna (Italy) between 2003
391 and 2008, J. Geophys. Res. 117, B07208, doi:10.1029/2011JB009114.
392 Caporali, A., Aichhorn, C., Barlik, M., Becker, M., Fejes, I., Gerhatova, L., Virag, G., 2009.
393 Surface kinematics in the Alpine–Carpathian–Dinaric and Balkan region inferred from a new
394 multi-network GPS combination solution. Tectonophysics 474(1), 295-321.
395 Catalano, S., Torrisi, S., Tortorici, G., Romagnoli, G., 2011. Active folding along a rift-flank: The
396 Catania region case history (SE Sicily). J. Geodynamics 51, 53–63.
397 Chiarabba, C., De Gori, P., Speranza, F., 2004. The southern Tyrrhenian subduction zone: Deep
398 geometry,magmatism and Plio-Pleistocene evolution, Earth Planet. Sci. Lett. 268 408-423, 2008.

399 Cianetti, S., Giunchi, C., Casarotti, E., 2012. Volcanic deformation and flank instability due to
400 magmatic sources and frictional rheology: the case of Mount Etna. Geophys. J. Int. 191 (3), 939-
401 953, doi:10.1111/j.1365-246X.2012.05689.x.
402 Cocina, O., Neri, G., Privitera, E., Spampinato, S., 1997. Stress tensor computation in the Mount
403 Etna area and tectonic implications. J. Geodynamics, 23, 109-127.
404 DISS Working Group 2010. Database of Individual Seismogenic Sources (DISS), Version 3.1.1: A
405 compilation of potential sources for earthquakes larger than M 5.5 in Italy and surrounding areas.
406 http://diss.rm.ingv.it/diss/, © INGV 2010 – Istituto Nazionale di Geofisica e Vulcanologia,
407 Doi:10.6092/INGV.IT-DISS3.1.1.
408 Ferranti, L., Oldow, J.S., D'Argenio, B., Catalano, R., Lewis, D., Marsella, E., Avellone, G.,
409 Maschio, L., Pappone, G., Pepe, F., Sulli, A., 2008. Active deformation in Southern Italy, Sicily
410 and southern Sardinia from GPS velocities of the Pery-Tyrrhenian Geodetic Array (PTGA). Boll.
411 Soc. Geol. It. 127 (2), 229-316.
412 Gambino, S., Mostaccio, A., Patanè, D., Scarfì, L., Ursino, A., 2004.-High-precision locations of
413 the microseismicity preceding the 2002–2003 Mt. Etna eruption. Geophys. Res. Lett. 31,
414 L18604, doi:10.1029/2004GL020499.
415 Gephart, J. W., 1990. - Stress and the direction of slip on fault planes, Tectonics 9 (4), 845–858.
416 Gephart, J.W., Forsyth D. W., 1984. An improved method for determining the regional stress tensor
417 using earthquake focal mechanism data: application to the San Fernando earthquake sequence, J.
418 Geophys. Res. 89, B11, 9305–9320.
419 Gillard, D., Wyss, M., Okubo, P., 1996. Type of faulting and orientation of stress and strain as a
420 function of space and time in Kilauea's south flank, Hawaii. J. Geophys. Res. 101, 16025–16042.
421 Giampiccolo, E., D'Amico, S., Patanè, D., Gresta, S., 2007. Attenuation and source parameters of
422 shallow micro earthquakes at Mt. Etna Volcano, Italy. Bull. of the Seismol. Soc. of Am. 97 (1B),
423 184-197.

Gruppo Analisi Dati, 2015. Catalogo dei terremoti della Sicilia Orientale–Calabria Meridionale (1999–2012). INGV - Catania (http://www.ct.ingv.it/ufs/analisti/catalogolist.php).

Herring, T.A., King, R.W., Mc Clusky, S.C., 2010. Introduction to GAMIT/GLOBK, Release 576 10.4, MIT, Cambridge, MA, 48pp.

Hollenstein, C. H., Kahle, H.G., Geiger, A., Jenny, S., Goes, S., Giardini D., 2003. New GPS constraints on the Africa-Eurasia plate boundary zone in southern Italy. Geophys. Res. Lett. 30(18), 1935, doi:10.1029/2003GL017554.

Huang, M.H., Hu, J.C., Hsieh, C.S., Ching, K.E., Rau, R.J., Pathier, E., Fruneau, B., Deffontaines, B., 2006. A growing structure near the deformation front in SW Taiwan as deduced from SAR interferometry and geodetic observation. Geophys. Res. Lett. 33, L12305, doi:10.1029/2005GL025613.

Labaume, P., Bousquet, J.C., Lanzafame, G. , 1990. Early deformation at a submarine compressive front: the Quaternary Catania foredeep south of Mt. Etna, Sicily, Italy. Tectonophysics 177, 349-366.

Lavecchia G., Ferrarini F., De Nardis R., Visini F., Barbano M.S. 2007. Active thrusting as a possible seismogenic source in Sicily (Southern Italy): Some insights from integrated structural-kinematic and seismological data. Tectonophysics 445, 145-167.

Lundgren, P., Casu, F., Manzo, M., Pepe, A., Berardino, P., Sansosti, E., Lanari, R., 2004. Gravity and magma induced spreading of Mount Etna volcano revealed by satellite radar interferometry. Geophys. Res. Lett. 31, L04602, doi:10.1029/2003GL018736.

Mayer, L., 1990. Introduction to Quantitative Geomorphology: An Exercise Manual. Englewood Cliffs, NJ, Prentice Hall.

Mattia, M., Bruno, V., Cannavò, F., Palano, M., 2012. Evidences of a contractional pattern along the northern rim of the Hyblean Plateau (Sicily, Italy) from GPS data. Geol. Acta 10, 1–9.

Michael, A. J. 1987. Use of focal mechanisms to determine stress: a control study, J. Geophys. Res. 92, B1, 357–368.

450 Monaco, C., Mazzoli, S., Tortorici, L., 1996. Active thrust tectonics in western Sicily (southern
451 Italy): the 1968 earthquake sequence. Terra Nova 8, 372-381.
452 Monaco, C., Tapponnier, P., Tortorici, L., Gillot, P.Y., 1997. Late Quaternary slip rates on the
453 Acireale-Piedimonte normal faults and tectonic origin of Mt. Etna (Sicily). E.P.S.L. 147, 125-
454 139.
455 Monaco, C., Catalano, S., De Guidi, G., Gresta, S., Langer, H., Tortorici, L., 2000. The geological
456 map of the urban area of Catania (eastern Sicily): morphotectonic and seismotectonic
457 implications. Mem. Soc. Geol. It. 55, 425-438.
458 Monaco, C., Tortorici, L., 2000. Active faulting in the Calabrian arc and eastern Sicily. J.
459 Geodynamics 29, 407-424.
460 Monaco, C., Bianca, M., Catalano, S., De Guidi, G., Tortorici, L., 2002. Sudden change in the Late
461 Quaternary tectonic regime in eastern Sicily: evidences from geological and geomorphological
462 features. Boll. Soc. Geol. It.121 (1), 901-913.
463 Monaco, C., De Guidi, G., Ferlito, C., 2010. The Morphotectonic map of Mt. Etna. Ital. J. Geosci.
464 129, 408-428.
465 Musumeci, C., Scarfì, L., Palano, M., Patanè, D., 2014. Foreland segmentation along an active
466 convergent margin: new constraints in southeastern Sicily (Italy) from seismic and geodetic
467 observations. Tectonophysics doi:org/10.1016/j.tecto.2014.05.017.
468 Neri, G., Barberi, G., Oliva, G. Orecchio, B., 2005. Spatial variations of seismogenic stress
469 orientations in Sicily, south Italy. Phys. of the Earth and Planet. Int. 148, 175–191.
470 Palano, M., Rossi, M., Cannavò, F., Bruno, V., Aloisi, M., Pellegrino, D., Pulvirenti, M., Siligato,
471 G., Mattia, M., 2010. Etn@ref: a geodetic reference frame for Mt. Etna GPS networks. Ann. of
472 Geophys. 53, 4, doi: 10.4401/ag-4879.
473 Palano, M., Ferranti, L., Mattia, M., Monaco, C., Aloisi, M., Bruno, V., Cannavò, F., Siligato, G.
474 2012. GPS velocity and strain fields in Sicily and southern Calabria, Italy: updated geodetic

475 constraints on tectonic block interaction in the central Mediterranean. J. Geophys. Res. 117, 1-
476 12.
477 Nishimura, T., Tobita, M., Yarai, H., Amagai, T., Fujiwara, M., Une, H., Koarai, M., 2008.
478 Episodic growth of fault-related fold in northern Japan observed by SAR interferometry.
479 Geophys. Res. Lett. 35, L13301, doi:10.1029/2008GL034337.
480 Patanè, D., Privitera, E., 2001. Seismicity related to 1989 and 1991-93 Mt. Etna (Italy) eruptions:
481 kinematic constraints by FPS analysis. J. Volcanol. Geotherm. Res. 109, 77-98.
482 Patanè, D., Barberi, G., Cocina, O., De Gori, P., Chiarabba, C., 2006. Time-Resolved Seismic
483 Tomography Detects Magma Intrusions at Mount Etna. Science 313, 821-823.
484 Pike, R.J., Wilson, S.E. 1971. Elevation-relief ratio, hypsometric integral, and geomorphic area-
485 altitude analysis. Geol. Soc. of Am. Bull. 82, 1079-1084.
486 Ragg, S., Grasso, M., Muller, B., 1999. Patterns of tectonic stress in Sicily from borehole breakout
487 observations and finite element modeling. Tectonics 18 (4), 669–685.
488 Reasenberg, P., Oppenheimer, D., 1985. FPFIT, FPPLOT, and FPPAGE: FORTRAN computer
489 programs for calculating and displaying fault plane solutions. U.S. Geol. Surv. Open File Rep.,
490 85/739, 109 pp.
491 Ristuccia, G.M., Di Stefano, A., Gueli, A.M., Monaco, C., Stella, G., Troja, S.O., 2013. OSL
492 chronology of Quaternary terraced deposits outcropping between Mt. Etna volcano and the
493 Catania Plain (Sicily, southern Italy). Phys. and Chem. of the Earth 63, 36-46.
494 Scarfì, L., Messina, A., Cassisi, C., 2013. Sicily and Southern Calabria focal mechanism database: a
495 valuable tool for the local and regional stress field determination. Ann. Geophys. 56, 1, D0109,
496 doi:10.4401/ag-6109.
497 Serpelloni, E., Vannucci, G., Pondrelli, S., Argnani, A., Casula, G., Anzidei, M., Baldi, P.,
498 Gasperini, P., 2007. Kinematics of the Western Africa-Eurasia plate boundary from focal
499 mechanisms and GPS data, Geophys. J. Int. 169, 1180-1200.

500 Sgroi, T., De Nardis, R., Lavecchia, G., 2012. Crustal structure and seismotectonicsof central Sicily
501 (southern Italy): new constraints from instrumental seismicity. Geophys. J. Int. 189, 1237–1252.
502 Shumm, S. A., 1956. Evolution of drainage system and slopes in badlands at Perth Amboy, New
503 Jersey. Geol. Soc. Am. Bull. 67, 655-668.
504 Solaro, G., Acocella, V., Pepe, S., Ruch, J., Neri, M., Sansosti, E., 2010. Anatomy of an unstable
505 volcano from InSAR: Multiple processes affecting flank instability at Mt. Etna, 1994–2008. J.
506 Geophys. Res. 115, B10405, doi:10.1029/2009JB000820.
507 Storti, F., Poblet, J. 1997. Growth stratal architectures associated to decollement folds and fault-
508 propagation folds. Inferences on fold kinematics. Tectonophysics 282 (1), 353-373.
509 Strahler, A. N., 1964. Quantitative geomorphology of drainage basins and channel networks. In
510 Chow, V.T. (ed), Handbook of Applied Hydrology, McGraw-Hill, New York, 439-476.
511 Torelli, L., Grasso, M., Mazzoldi, G., Peis, D., 1998. Plio–Quaternary tectonic evolution and
512 structure of the Catania foredeep, the northern Hyblean Plateau and the Ionian shelf (SE Sicily).
513 Tectonophysics 298 209–221.
514 Wyss, M., Liang, B., Tanigawa, W.R., Wu, X., 1992. Comparison of the orientation of stress and
515 strain tensors based on fault plane solutions in Kaoiki, Hawaii, J. Geophys. Res. 97, 4769–4790.
516 Zhang, H., Thurber, C., Bedrosian, P., 2009. Joint inversion for Vp, Vs, and Vp/Vs at SAFOD,
517 Parkfield, California. Geochem. Geophys. Geosyst. 10:Q110032, doi:10.1029/2009GC002709.

518 **FIGURE CAPTIONS**

519

520 Fig.1. Seismotectonic map of Mt. Etna region; earthquakes recorded during the period 1994-2012
521 are reported. Inset: Tectonic sketch map of central Mediterranean.

522

523 Fig. 2. Crustal section with projection of the hypocentral distribution and structural interpretation
524 (Moho depth from Lavecchia et al., 2007 and references therein). For the trace of section see Fig.1.

525

526 Fig.3. Focal solutions (on the left) and P-axes orientations (on the right) for three different depth
527 intervals.

528

529 Fig. 4. Orientations (lower-hemisphere projection) of the principal stress axes obtained by inverting
530 the FPSsin three sub-areas (N, C, S). Red circles show the related earthquake locations. Grey areas
531 indicate the 95% confidence limits of σ_1 and σ_3 orientations.

532

533 Fig. 5. Horizontal GPS velocities (1994–2013) with 95% confidence ellipses in the Eurasian
534 reference frame (Altamimi et al., 2007) for the measured IGM benchmarks located close to the
535 Catania anticline.

536

537 Fig. 6. Geological-structural map of lower southern flank of Mt. Etna.

538

539 Fig. 7. a) Morphological map of the analysed area (2x2 m grid DEM from
540 www.sitr.regione.sicilia.it/pai). Morphometric analysis was carried out on evidenced drainage
541 basins; b) hypsometric curves of analysed drainage basins and geological section along the fold axis
542 of the Catania anticline.

543

544 Fig. 8. Schematic representation of a possible low-angle blind thrust (detachment and fold) at the
545 frontal and shallow part of the SBT (see text for discussion).
546
547 Tab. 1. Seismogenic Stress Tensor: N, F and R are, respectively, the number of events, the average
548 misfit corresponding to the stress solution found and the measure of relative stress magnitude. Dip
549 and strike of the maximum (σ_1), intermediate (σ_2) and minimum (σ_3) compressive stress axes are
550 reported.
551
552 Tab. 2. Morphometric parameters obtained by the analysis of drainage basins interacting with the
553 active deformation zone.
554

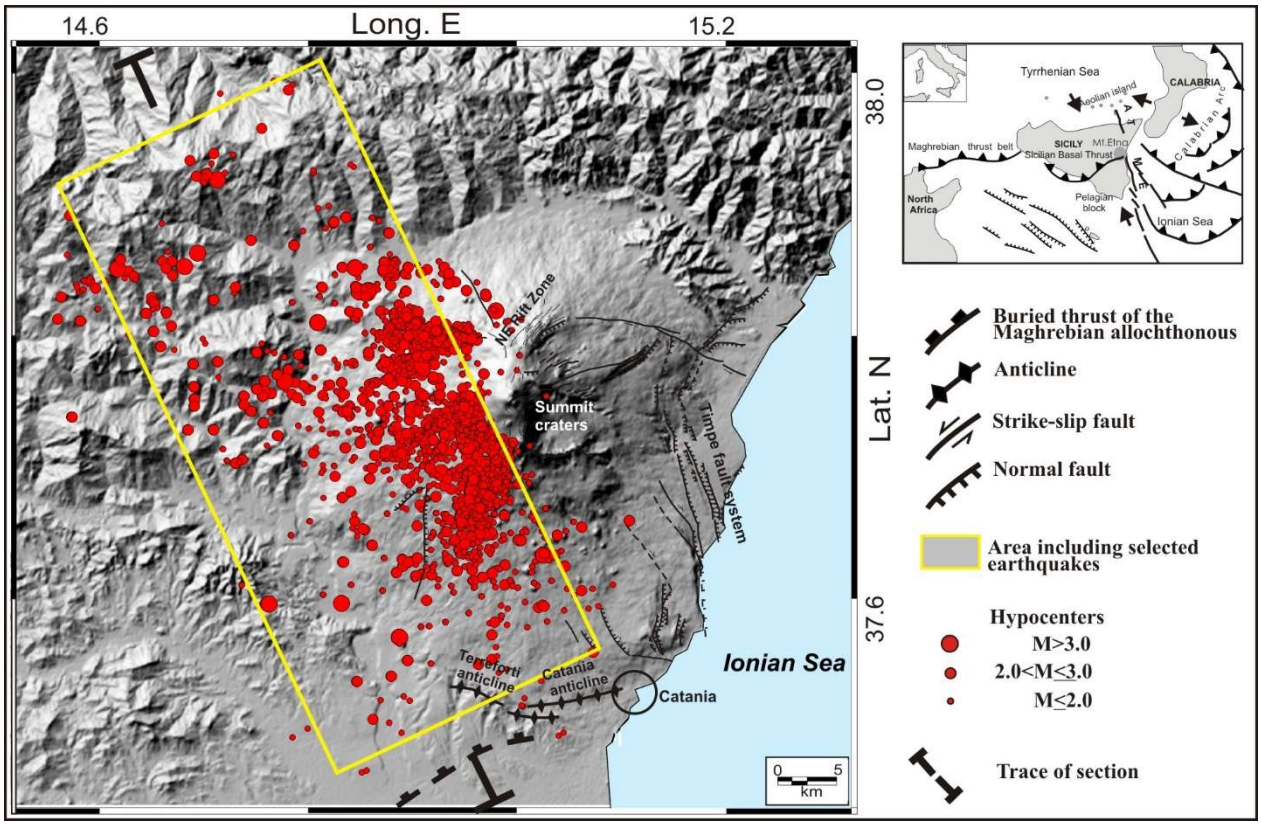

555

556 Fig.1. Seismotectonic map of Mt. Etna region; earthquakes recorded during the period 1994-2012

557 are reported. Inset: Tectonic sketch map of central Mediterranean.

558

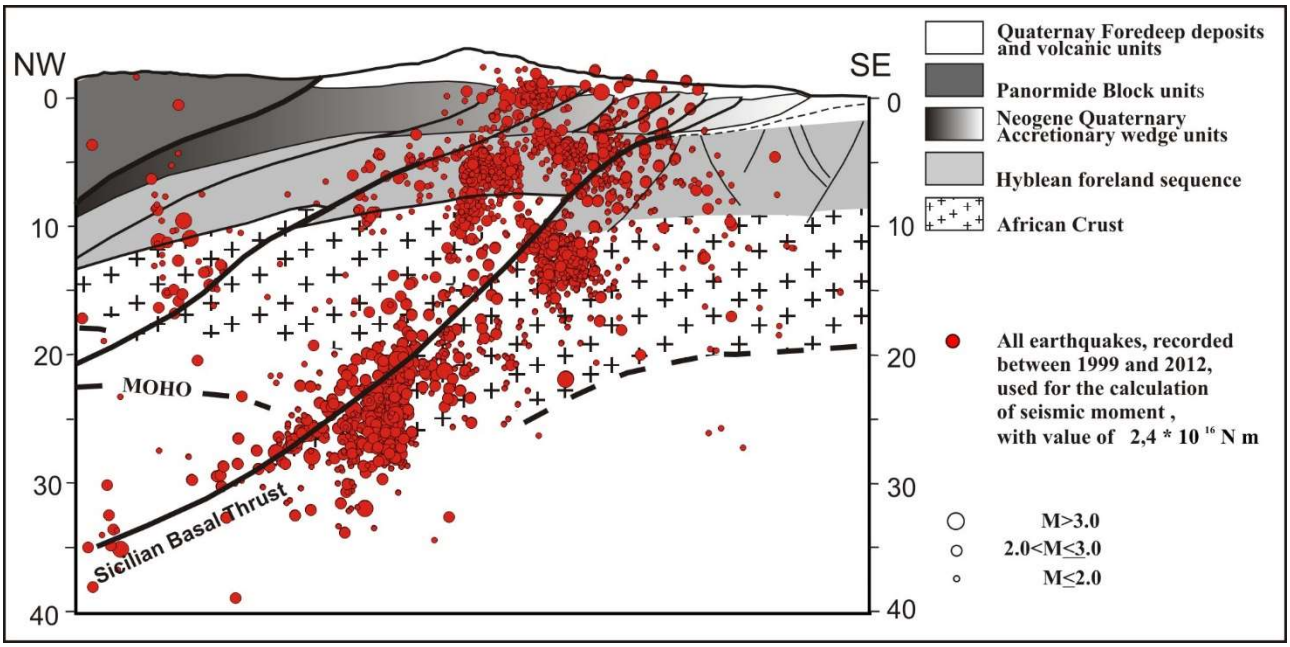

559

560 Fig. 2. Crustal section with projection of the hypocentral distribution and structural interpretation

561 (Moho depth from Lavecchia et al., 2007 and references therein). For the trace of section see Fig.1.

562

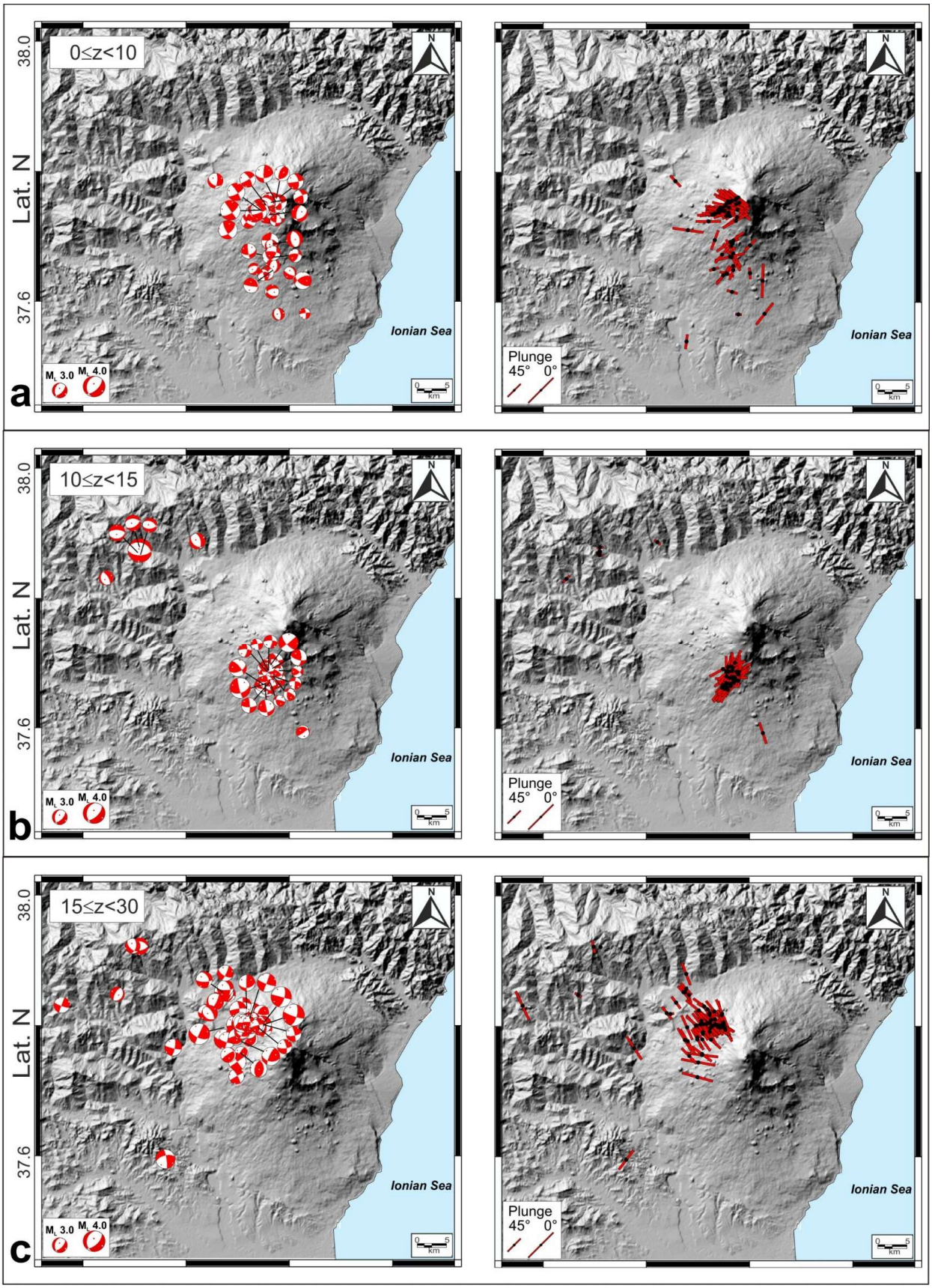

Fig.3. Focal solutions (on the left) and P-axes orientations (on the right) for three different depth intervals.

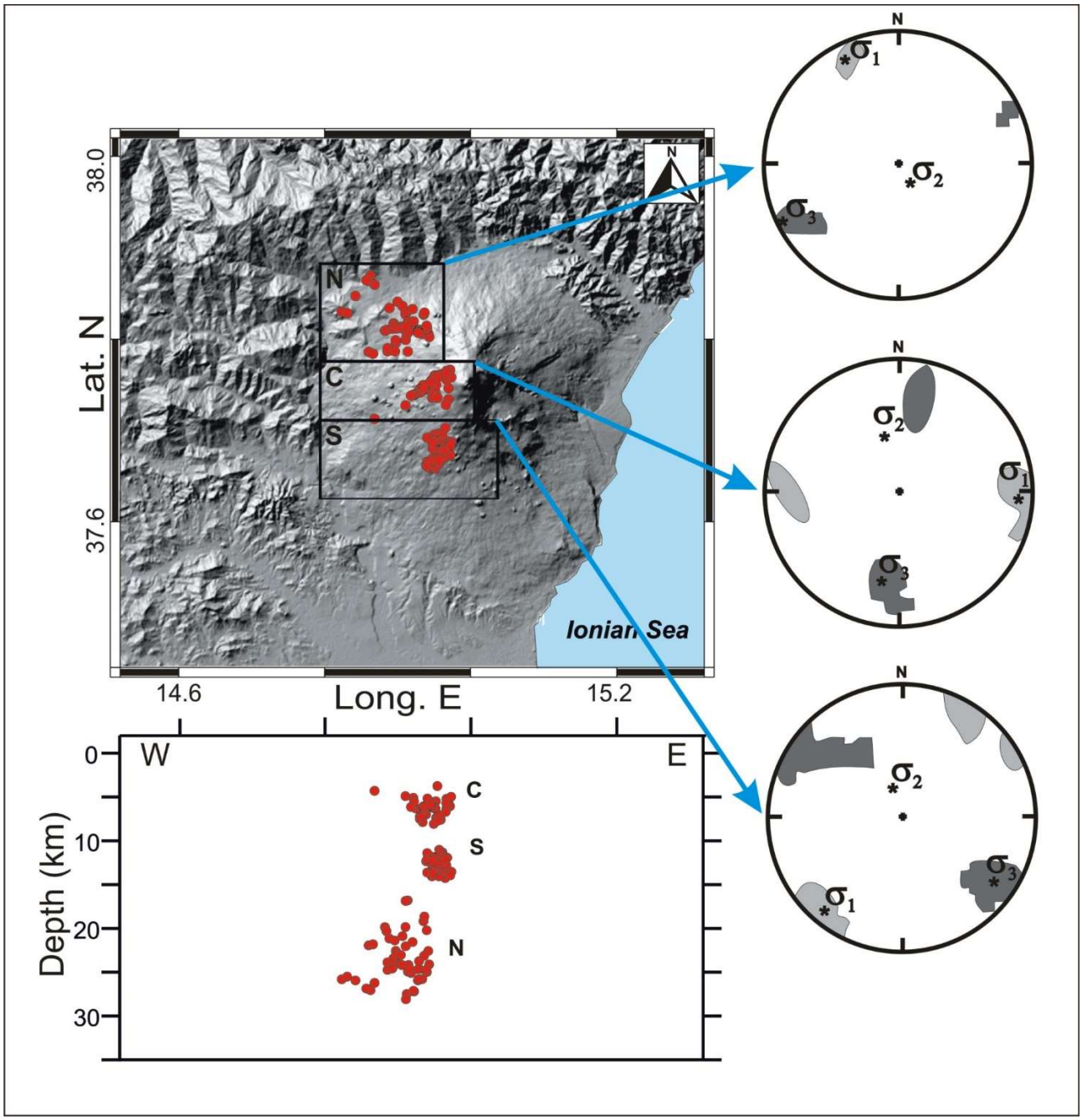

Fig. 4. Orientations (lower-hemisphere projection) of the principal stress axes obtained by inverting the FPSsin three sub-areas (N, C, S). Red circles show the related earthquake locations. Grey areas indicate the 95% confidence limits of σ_1 and σ_3 orientations.

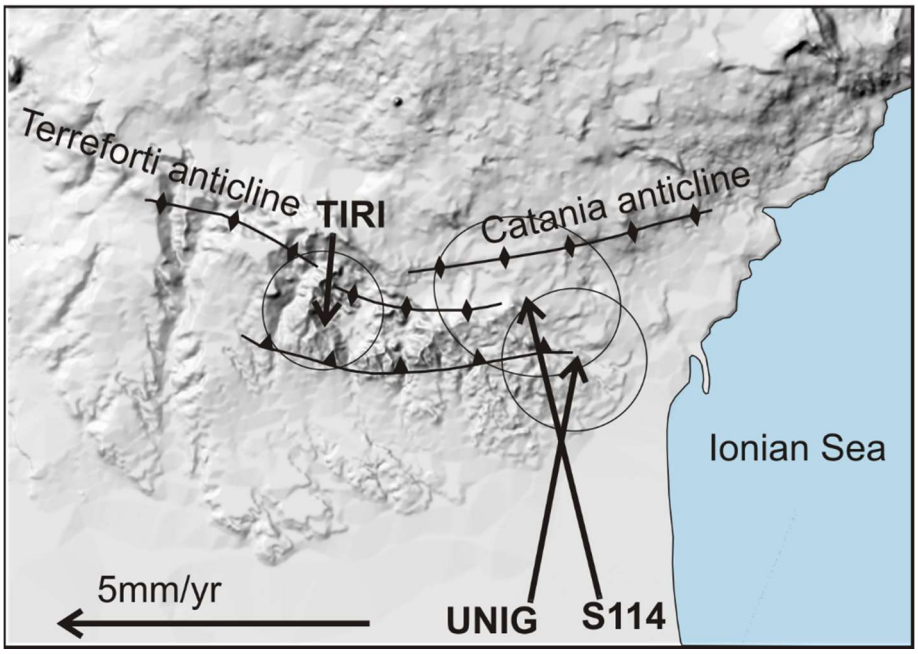

571

572 Fig. 5. Horizontal GPS velocities (1994–2013) with 95% confidence ellipses in the Eurasian
573 reference frame (Altamimi et al., 2007) for the measured IGM benchmarks located close to the
574 Catania anticline.

575

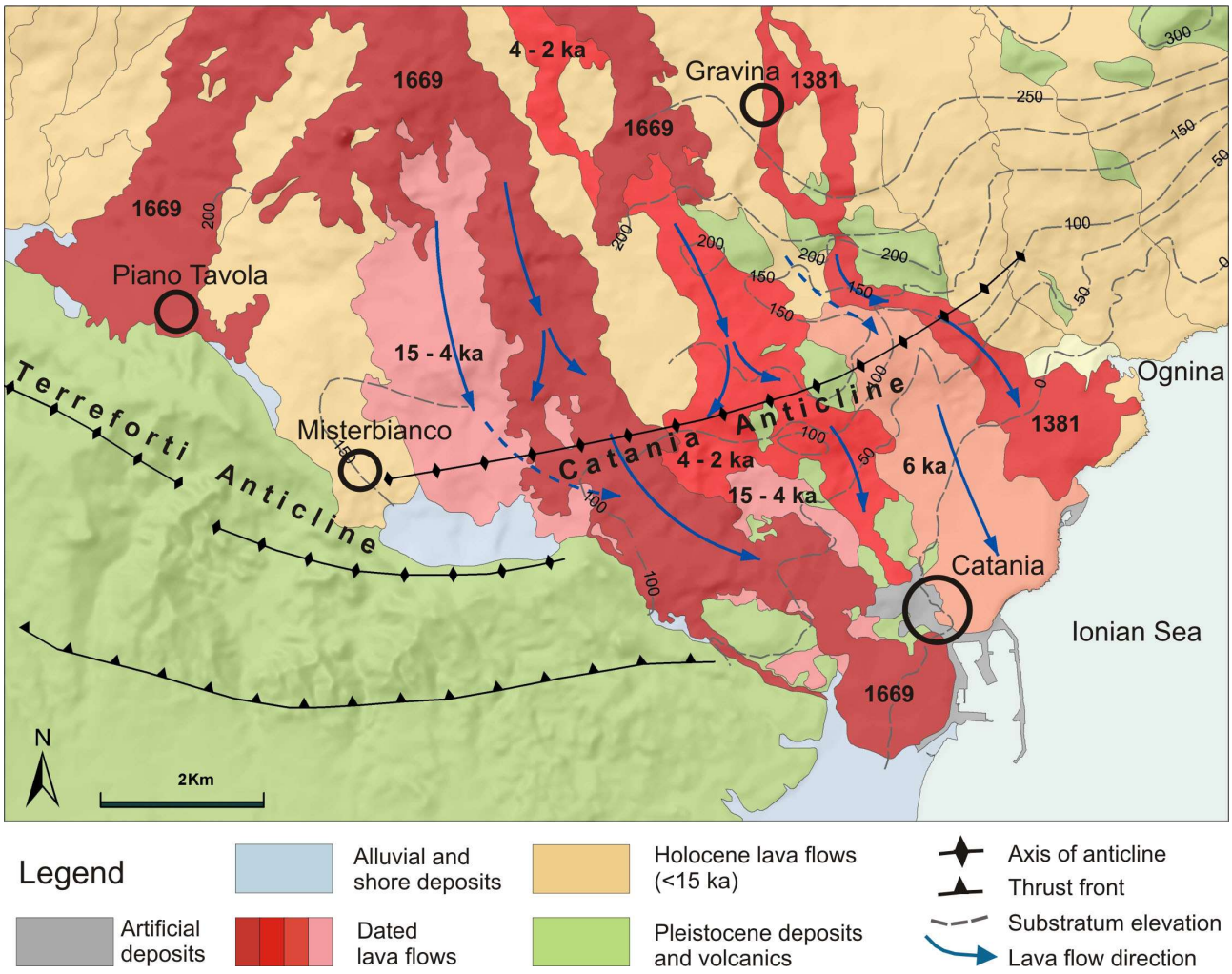

Fig. 6. Geological-structural map of lower southern flank of Mt. Etna.

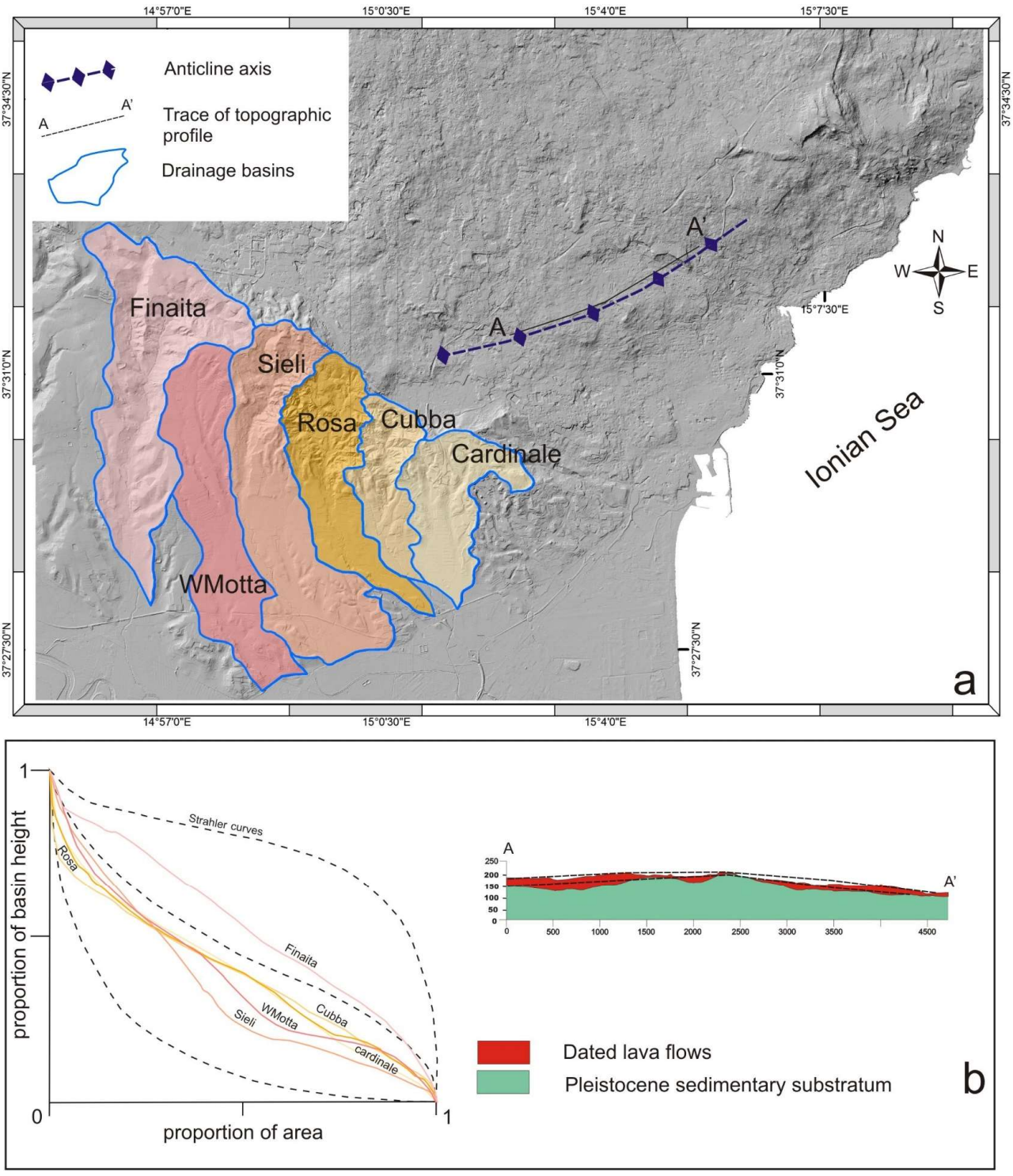

Fig. 7. a) Morphological map of the analysed area (2x2 m grid DEM from www.sitr.regione.sicilia.it/pai). Morphometric analysis was carried out on evidenced drainage basins; b) hypsometric curves of analysed drainage basins and geological section along the fold axis of the Catania anticline.

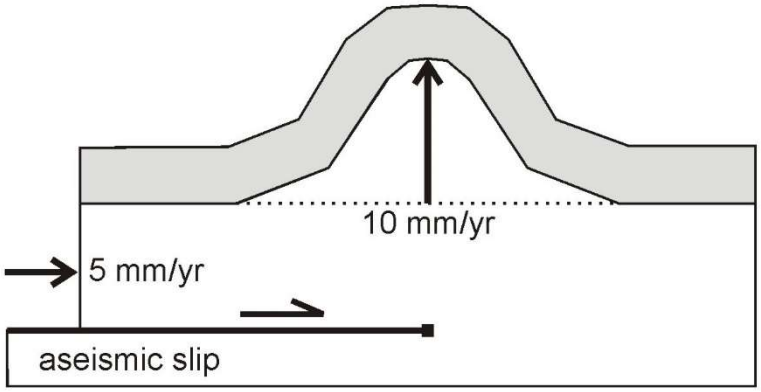

585

586 Fig. 8. Schematic representation of a possible low-angle blind thrust (detachment and fold) at the

587 frontal and shallow part of the SBT (see text for discussion).

588

Table 1

Dataset	N	F(°)	R	σ_1		σ_2		σ_3	
				Dip	Strike	Dip	Strike	Dip	Strike
N	52	4.2	0.7	14	333	76	147	1	243
C	41	5.9	0.5	12	93	54	346	33	191
S	45	5.4	0.6	10	219	71	341	16	126

Tab. 1. Seismogenic Stress Tensor: N, F and R are, respectively, the number of events, the average misfit corresponding to the stress solution found and the measure of relative stress magnitude. Dip and strike of the maximum (σ_1), intermediate (σ_2) and minimum (σ_3) compressive stress axes are reported.

Table 2

Basin	Length (m)	Average width (m)	Area (m^2)	Eb
Cardinale	4011	1200	6416984	0.71
Cubba	5093	1000	4634778	0.41
Rosa	7538	1000	8243513	0.42
Sieli	9574	1450	14196713	0.24
Motta	6657	1300	10983604	0.56
Finaita	9726	1250	14783289	0.44

Tab. 2. Morphometric parameters obtained by the analysis of drainage basins interacting with the active deformation zone.